Influence of strong coupling and pulse delay in a system involving double autoionization resonance

Takashi Nakajima
Institute of Advanced Energy, Kyoto University, Gokasho, Uji, Kyoto 611-0011, Japan
(Received 14 June 1999)

We study the dynamics of a system involving double autoionization resonance. We find that a strong dipole coupling between two autoionizing states significantly modifies the properties of the medium. Variation of the linear susceptibility and ionization spectra into each continuum are numerically calculated for illustration. Effects of the temporal delay between pulses are also investigated in terms of the ionization yield into each continuum. [S1050-2947(99)09212-4]

PACS number(s): 42.50.Hz, 32.80.Rm, 32.80.Qk, 42.65.An

I. INTRODUCTION

When a three-level system interacts with two lasers having frequencies close to the transition frequencies of initial-intermediate states and intermediate-final states, it is said that the system is in a double resonance. Most well-known effects in such a system are ac Stark splitting and coherent population trapping [1,2]. Various interesting phenomena associated with these effects have been found theoretically as well as experimentally in the last several years, some of which are lasing without inversion [3], electromagnetically induced transparency [4], and coherent population transfer [5]. It should be noted that a bound three-level system has been the vehicle for these studies. For a system involving a continuum, an interesting phenomenon has been found, which is known nowadays as laser-induced continuum structure (LICS). Theoretical and experimental study of LICS has been performed by several groups [6–10].

When it comes to a system involving one or more autoionizing states, however, there are not many works in the literature. The main difference between a bound-state system and an autoionizing system is that, for the former coherence is generated only through interactions with lasers, while for the latter there exists intrinsic coherence due to the electrostatic interaction, or configuration interaction, even without laser fields. Therefore more interesting effects due to the interplay of *laser-induced coherence* and *intrinsic coherence* is to be expected in such systems. An original work of autoionizing states in strong laser fields has been done by Lambropoulos and Zoller [11]. Gallagher *et al.* [12] have used the double resonance via autoionization states for a selective pumping to the higher autoionizing state (HAS). Zhang and van Enk [13] have used a similar idea for a theoretical study of above-threshold ionization and third-harmonic generation through an autoionization resonance. More recently Karapanagioti *et al.* [14,15] have studied the effects of the strong coupling between two autoionizing states by a laser in terms of the ionization yield.

In this paper we study the effects of strong coupling and temporal delay between two pulses in a system involving two autoionizing states under double resonance. The purpose is to investigate the difference as well as the similarity of the effects with those found in a bound three-level system. It should be noted that, when the interaction of an atomic system and short-wavelength lasers is to be examined, the states above ionization threshold necessarily need to be taken into account. Thus a study of an autoionizing system would be relevant from this context as well, in order to explore the possibility of applying the ideas, found for bound-state systems, in the shorter wavelength region. In particular, we focus on the variation of linear susceptibility, ionization yield into each continuum with laser detunings and intensities as controlling parameters, and the effects of the temporal pulse delay in terms of the excitation (ionization) efficiency.

First of all, as for the linear susceptibility, Scully and co-workers [16–18] have theoretically found that an incoherent pumping is essential in order for bound-state systems to exhibit an enhanced index of refraction near an atomic resonance while canceling the absorption. With the use of an appropriate autoionizing medium, however, there is no need of introducing any complicated pumping mechanism for that, as we point out in this paper. Such a property of an autoionizing medium has been implicit in the literature, but to our knowledge there is no work focusing on this issue. Second, for controlled excitation into each autoionizing state with a proper choice of laser parameters such as detunings and intensities, Gallagher *et al.* [12] have employed the absorption minimum of the lower autoionizing state (LAS) for a selective pumping to the HAS. They considered the system within a transition rate picture, or weak-field limit. It is not known what will happen when the laser coupling is sufficiently strong. In this paper we investigate the effects of the detunings and coupling strength beyond the weak-field limit. A set of density-matrix equations is employed for that. Third, about the pulse delay effects, it is well known for a bound three-level system that a counterintuitive pulse delay significantly enhances the population transfer efficiency from an initially occupied state to an initially unoccupied final state [5]. Recently we have reported the effects of the pulse delay for the cases in which the intermediate state is replaced by a continuum [19] and an autoionizing state [20]. It should be noted that, as its further variants, the mechanism of population transfer in N-level systems [21–23], and selective population transfer in a multilevel system [24] have recently been reported. In this paper we also examine the effects of the pulse delay when not only the intermediate state but also the final one is an autoionizing state.

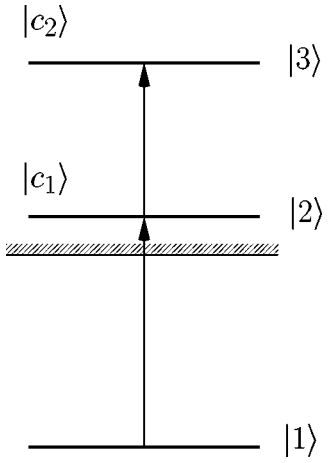

FIG. 1. Level scheme studied in this paper. Discrete states $|2\rangle$ and $|3\rangle$ lie above ionization thresholds and interact with the continua $|c_1\rangle$ and $|c_2\rangle$.

II. MODEL

A. Basic equations

We consider the system shown in Fig. 1. A bound state $|1\rangle$ and a discrete state $|2\rangle$, and $|2\rangle$ and another discrete state $|3\rangle$ are coupled by two lasers, respectively. The discrete states $|2\rangle$ and $|3\rangle$ are embedded in continua $|c_1\rangle$ and $|c_2\rangle$, respectively, and coupled to them through configuration interaction V. Following the standard procedure [11], we find that this system is governed by a set of density-matrix equations given below,

$$\dot{\sigma}_{11}=-\gamma_1\sigma_{11}+2\,\mathrm{Im}\left[\Omega_1\left(1-\frac{i}{q_1}\right)\sigma_{21}\right], \tag{1}$$

$$\dot{\sigma}_{22}=-(\gamma_2+\Gamma_2)\sigma_{22}-2\,\mathrm{Im}\left[\Omega_1\left(1+\frac{i}{q_1}\right)\sigma_{21}\right]+2\,\mathrm{Im}\left[\Omega_2\left(1-\frac{i}{q_2}\right)\sigma_{32}\right], \tag{2}$$

$$\dot{\sigma}_{33}=-(\gamma_3+\Gamma_3)\sigma_{33}-2\,\mathrm{Im}\left[\Omega_2\left(1+\frac{i}{q_2}\right)\sigma_{32}\right], \tag{3}$$

$$\dot{\sigma}_{21}=\left[i\delta_1-\frac{1}{2}(\gamma_1+\gamma_2+\Gamma_2)\right]\sigma_{21}-i\Omega_1\left(1-\frac{i}{q_1}\right)\sigma_{11}+i\Omega_1\left(1+\frac{i}{q_1}\right)\sigma_{22}-i\Omega_2\left(1-\frac{i}{q_2}\right)\sigma_{31}, \tag{4}$$

$$\dot{\sigma}_{31}=\left[i(\delta_1+\delta_2)-\frac{1}{2}(\gamma_1+\gamma_3+\Gamma_3)\right]\sigma_{31}-i\Omega_2\left(1-\frac{i}{q_2}\right)\sigma_{21}+i\Omega_1\left(1+\frac{i}{q_1}\right)\sigma_{32}, \tag{5}$$

$$\dot{\sigma}_{32}=\left[i\delta_2-\frac{1}{2}(\gamma_2+\gamma_3+\Gamma_2+\Gamma_3)\right]\sigma_{32}-i\Omega_2\left(1-\frac{i}{q_2}\right)\sigma_{22}+i\Omega_2\left(1+\frac{i}{q_2}\right)\sigma_{33}+i\Omega_1\left(1+\frac{i}{q_1}\right)\sigma_{31}, \tag{6}$$

where γ_1, γ_2, and γ_3 describe the direct photoionization widths from states $|1\rangle$, $|2\rangle$, and $|3\rangle$ into the associated continua, respectively, while Γ_2 and Γ_3 stand for the autoionization widths from states $|2\rangle$ and $|3\rangle$. $\Omega_j(1-i/q_j)$ $(j=1,2)$ are the complex Rabi frequencies between $|1\rangle$ and $|2\rangle$, and $|2\rangle$ and $|3\rangle$, respectively. It should be noted that the Rabi frequencies between a bound and an autoionizing state, or two autoionizing states become complex after the pole approximation due to the presence of the continuum. δ_1 and δ_2 are the laser detunings, and the parameters q_j $(j=1,2)$, which characterize the degree of asymmetry in ionization profiles, have been defined as

$$q_1=\frac{2\Omega_1}{\sqrt{\gamma_1\Gamma_2}}, \tag{7}$$

$$q_2=\frac{2\Omega_2}{\sqrt{\Gamma_2\gamma_3}+\sqrt{\gamma_2\Gamma_3}}. \tag{8}$$

After the slowly varying envelope approximation, the polarization components with frequency ω_1 are obtained, in terms of the density-matrix elements σ_{21} and $\sigma_{c_1 1}$ [already eliminated in Eqs. (1)–(6)], as

$$P_1=\left(\mu_{12}\sigma_{21}+\sum_{c_1}\mu_{1c_1}\sigma_{c_1 1}\right)+\text{c.c.}$$

$$=\left(s_1'-i\frac{\gamma_1'}{2}\right)\varepsilon_1\sigma_{11}+\mu_{12}\left(1-\frac{i}{q_1}\right)\sigma_{21}+\text{c.c.}, \tag{9}$$

where ε_1 is the field amplitude of the first laser, and μ_{12} and μ_{1c_1} are the dipole matrix elements between $|1\rangle$ and $|2\rangle$, and $|1\rangle$ and $|c_1\rangle$, respectively. In the above equation, s_1 and γ_1 have been defined as

$$s_1'-\frac{i}{2}\gamma_1'=\sum_{c_1}\frac{|\mu_{1c_1}|^2}{\delta_{c_1}}, \tag{10}$$

with δ_{c_1} being the detuning from the resonant energy. Although Eqs. (1)–(6) can be solved numerically without any difficulty, it would be useful to derive analytical expressions for the linear susceptibility χ. Assuming a weak pumping, it is valid to set $\sigma_{11}^{(0)}\sim 1$ and $\sigma_{22}^{(0)}=\sigma_{33}^{(0)}\sim 0$ in Eqs. (4)–(6) to the zeroth order in the field amplitude ε_1. Then these equations can be solved for a steady state, and the off-diagonal elements σ_{21} and σ_{31} are obtained, to the first order in the field amplitude ε_1 and all orders in ε_2, as

$$\sigma_{21}^{(1)}=-\frac{i\Omega_1\left(1-\frac{i}{q_1}\right)\left[-i(\delta_1+\delta_2)+\frac{1}{2}(\gamma_1+\gamma_3+\Gamma_3)\right]}{\left[-i\delta_1+\frac{1}{2}(\gamma_1+\gamma_2+\Gamma_2)\right]\left[-i(\delta_1+\delta_2)+\frac{1}{2}(\gamma_1+\gamma_3+\Gamma_3)\right]+\left[\Omega_2\left(1-\frac{i}{q_2}\right)\right]^2}, \tag{11}$$

$$\sigma_{31}^{(1)}=-\frac{\Omega_1\left(1-\frac{i}{q_1}\right)\Omega_2\left(1-\frac{i}{q_2}\right)}{\left[-i\delta_1+\frac{1}{2}(\gamma_1+\gamma_2+\Gamma_2)\right]\left[-i(\delta_1+\delta_2)+\frac{1}{2}(\gamma_1+\gamma_3+\Gamma_3)\right]+\left[\Omega_2\left(1-\frac{i}{q_2}\right)\right]^2}. \tag{12}$$

Hence the linear susceptibility χ is found as

$$\chi=\left(s_1'-i\frac{\gamma_1'}{2}\right)+\frac{\mu_{12}^2\left(1-\frac{i}{q_1}\right)^2\left[-i(\delta_1+\delta_2)+\frac{1}{2}(\gamma_1+\gamma_2)\right]}{\left[-i\delta_1+\frac{1}{2}(\gamma_1+\gamma_2+\Gamma_2)\right]\left[-i(\delta_1+\delta_2)+\frac{1}{2}(\gamma_1+\gamma_3+\Gamma_3)\right]+\left[\Omega_2\left(1-\frac{i}{q_2}\right)\right]^2}. \tag{13}$$

An expression of χ for a bound three-level system can be immediately obtained from the above expression just by setting $q_1=q_2=\infty$, $\gamma_1=\gamma_2=\gamma_3=0$, and $s_1=\gamma_1=0$. An expression of χ for the case in which one of the states $|2\rangle$ or $|3\rangle$ are bound can be obtained in a similar manner.

B. Ionization spectra

Equations (1)–(6) describe the dynamics of the system consisting of the bound state and the two autoionizing states. Although the total ionization yield R can be obtained by

$$R=1-\sum_{k=1}^{3}\sigma_{kk}, \tag{14}$$

ionization yield and photoelectron spectrum into each continuum $|c_j\rangle$ $(j=1,2)$ cannot be obtained from this equation. For that purpose, it is necessary to write down a set of density-matrix equations for continua $|c_j\rangle$ $(j=1,2)$, which reads

$$\dot{\sigma}_{c_1c_1}=-2\ \mathrm{Im}(D_{c_11}\sigma_{c_11})-2\ \mathrm{Im}(V_{c_12}\sigma_{c_12}), \tag{15}$$

$$\dot{\sigma}_{c_2c_2}=-2\ \mathrm{Im}(D_{c_22}\sigma_{c_22})-2\ \mathrm{Im}(V_{c_23}\sigma_{c_23}), \tag{16}$$

$$\dot{\sigma}_{c_11}=\left(i\delta_{c_1}-\frac{1}{2}\gamma_1\right)\sigma_{c_11}+i\Omega_1\left(1+\frac{i}{q_1}\right)\sigma_{c_12}-iD_{c_11}\sigma_{11}-iV_{c_12}\sigma_{21}, \tag{17}$$

$$\dot{\sigma}_{c_12}=\left[i(\delta_{c_1}-\delta_1)-\frac{1}{2}(\gamma_2+\Gamma_2)\right]\sigma_{c_12}+i\Omega_1\left(1+\frac{i}{q_1}\right)\sigma_{c_11}+i\Omega_2\left(1+\frac{i}{q_2}\right)\sigma_{c_13}-iD_{c_11}\sigma_{12}-iV_{c_12}\sigma_{22}, \tag{18}$$

$$\dot{\sigma}_{c_13}=\left[i(\delta_{c_1}-\delta_1-\delta_2)-\frac{1}{2}(\gamma_3+\Gamma_3)\right]\sigma_{c_13}+i\Omega_2\left(1+\frac{i}{q_2}\right)\sigma_{c_12}-iD_{c_11}\sigma_{13}-iV_{c_12}\sigma_{23}, \tag{19}$$

$$\dot{\sigma}_{c_21}=\left(i\delta_{c_2}-\frac{1}{2}\gamma_1\right)\sigma_{c_21}+i\Omega_1\left(1+\frac{i}{q_1}\right)\sigma_{c_22}-iD_{c_22}\sigma_{21}-iV_{c_23}\sigma_{31}, \tag{20}$$

$$\dot{\sigma}_{c_22}=\left[i(\delta_{c_2}-\delta_1)-\frac{1}{2}(\gamma_2+\Gamma_2)\right]\sigma_{c_12}+i\Omega_1\left(1+\frac{i}{q_1}\right)\sigma_{c_21}+i\Omega_2\left(1+\frac{i}{q_2}\right)\sigma_{c_23}-iD_{c_22}\sigma_{22}-iV_{c_23}\sigma_{32}, \tag{21}$$

$$\dot{\sigma}_{c_23}=\left[i(\delta_{c_2}-\delta_1-\delta_2)-\frac{1}{2}(\gamma_3+\Gamma_3)\right]\sigma_{c_23}+i\Omega_2\left(1+\frac{i}{q_2}\right)\sigma_{c_22}-iD_{c_22}\sigma_{23}-iV_{c_23}\sigma_{33}, \tag{22}$$

where $D_{c_j k}$ and $V_{c_j k}$ ($j=1$ or 2, $k=1$, 2, or 3) are bound-free and configuration-interaction matrix elements, respectively, which are related to the previously defined quantities through $\gamma_j = 2\pi |D_{c_j j}|^2$ ($j=1,2,3$), and $\Gamma_2 = 2\pi |V_{c_1 2}|^2$ and $\Gamma_3 = 2\pi |V_{c_2 3}|^2$. By introducing piecewise continuum states with energies E_{c_j} and solving the above set of equations together with those given in Eqs. (1)–(6), ionization yield R_1 and R_2 into each continuum $|c_j\rangle$ ($j=1,2$) can be obtained by integrating over the photoelectron energy as

$$R_j = \int_{-\infty}^{\infty} dE_{c_j} \sigma_{c_j c_j} \rho(E_{c_j}) \quad (j=1,2), \tag{23}$$

where $\rho(E_{c_j})$ is a density of states at energy E_{c_j}. When numerically solving Eqs. (1)–(6) and Eqs. (15)–(22), the number and the energy spacing of the discretized continua have been chosen so that the reasonable convergence is obtained, i.e., $\Sigma_{k=1}^{3} \sigma_{kk} + R_1 + R_2 \sim 1$ with numerical deviation less than 1%.

C. Reduced equations

In some cases it is useful to eliminate an unnecessary state from the system of interest. When each of the first and the second lasers are far-detuned from resonance but the two-photon frequency is still close to the $|1\rangle$-$|3\rangle$ transition, i.e., $|\delta_j| \gg \Gamma_j$ ($j=1,2$) but $|\delta_1 + \delta_2| \lesssim \Gamma_3$, state $|2\rangle$ may be adiabatically eliminated from Eqs. (1)–(6), and we obtain a set of reduced equations as

$$\dot{\sigma}_{11} = -(\gamma_1 + \tilde{\gamma}_1)\sigma_{11} + 2\,\mathrm{Im}\left[\frac{\Omega_1\left(1 - \frac{i}{q_1}\right)\Omega_2\left(1 - \frac{i}{q_2}\right)}{\delta_1 + \frac{i}{2}(\gamma_1 + \gamma_2 + \Gamma_2)} \sigma_{31} \right], \tag{24}$$

$$\dot{\sigma}_{33} = -(\gamma_3 + \Gamma_3 + \tilde{\gamma}_3)\sigma_{33} + 2\,\mathrm{Im}\left[\frac{\Omega_1\left(1 + \frac{i}{q_1}\right)\Omega_2\left(1 + \frac{i}{q_2}\right)}{\delta_2 + \frac{i}{2}(\gamma_2 + \gamma_3 + \Gamma_2 + \Gamma_3)} \sigma_{31} \right], \tag{25}$$

$$\dot{\sigma}_{31} = -i\left[\frac{\Omega_1\left(1 - \frac{i}{q_1}\right)\Omega_2\left(1 - \frac{i}{q_2}\right)}{\delta_1 + \frac{i}{2}(\gamma_1 + \gamma_2 + \Gamma_2)} \right] \sigma_{11} - i\left[\frac{\Omega_1\left(1 + \frac{i}{q_1}\right)\Omega_2\left(1 + \frac{i}{q_2}\right)}{\delta_2 + \frac{i}{2}(\gamma_2 + \gamma_3 + \Gamma_2 + \Gamma_3)} \right] \sigma_{33} + \left[i(\delta_1 + \delta_2 + \delta\omega_1 + \delta\omega_2) - \frac{1}{2}(\gamma_1 + \tilde{\gamma}_1 + \gamma_3 + \Gamma_3 + \tilde{\gamma}_3) \right] \sigma_{31}, \tag{26}$$

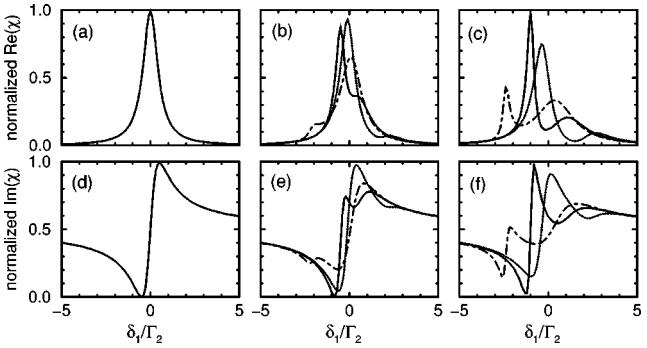

FIG. 2. Linear susceptibility χ as a function of δ_1/Γ_2 for $\delta_2/\Gamma_3 = -2$ (dotted), 0 (solid), and 2 (dot-dashed). $\Gamma_2 = \Gamma_3 = 1$ and $q_1 = 1$ and $q_2 = 2$. Graphs (a), (b), and (c) are real parts, and graphs (d), (e), and (f) are imaginary parts of the linear susceptibility at different Ω_2, respectively. Normalization has been made at the peak value of $Re(\chi)$ for $\Omega_2 = 0$ [graph (a)]. $\Omega_2 = 0$, $0.5\Gamma_3$, and Γ_3 for graphs (a) and (d), (b) and (e), and (c) and (f), respectively.

where

$$\delta\omega_1 + \frac{i}{2}\tilde{\gamma}_1 = -\frac{\left[\Omega_1\left(1 + \frac{i}{q_1}\right)\right]^2}{\delta_2 + \frac{i}{2}(\gamma_2 + \gamma_3 + \Gamma_2 + \Gamma_3)}, \tag{27}$$

$$\delta\omega_2 + \frac{i}{2}\tilde{\gamma}_3 = -\frac{\left[\Omega_2\left(1 - \frac{i}{q_2}\right)\right]^2}{\delta_1 + \frac{i}{2}(\gamma_1 + \gamma_2 + \Gamma_2)}. \tag{28}$$

$\tilde{\gamma}_1$ and $\tilde{\gamma}_3$ represent the additional ionizations from states $|1\rangle$ and $|3\rangle$ due to the excitation via the far wing of the eliminated state $|2\rangle$. $\delta\omega_1$ and $\delta\omega_2$ are quadratic shifts induced by the first and the second lasers, respectively. Note that this treatment is valid in the intensity region where the continuum-continuum and continuum-discrete transitions do not play a significant role, since we have neglected the couplings such as $|c_1\rangle$-$|c_2\rangle$ and $|c_1\rangle$-$|3\rangle$. In practice, the typical intensity below which our treatment is valid is about $\sim 10^{12}$ W/cm^2.

III. NUMERICAL EXAMPLES

A. Linear susceptibility

Figure 2 shows the profiles of the linear susceptibility χ for $q_1 = 1$ and $q_2 = 2$ at different intensities of the second laser, i.e., at different Ω_2, and different detunings δ_2/Γ_3. When $\Omega_2 = 0$ [Figs. 2(a) and 2(d)], the profile of χ is determined purely by the value of q_1. It can be seen that the profiles of the real and the imaginary parts of χ are very much different from those found in a bound-state system. Especially for $q_1 = 1$, the profiles of the real and the imaginary parts of χ, respectively, look like those of the imaginary and the real parts of a bound-state system. This is due to the intrinsic coherence of an autoionizing state. It is interesting to note that $\mathrm{Re}(\chi)$ does not change sign in this particular case as the detuning δ_1/Γ_2 crosses the resonance. As $|q_1|$ becomes large (not shown), the profile of each component of

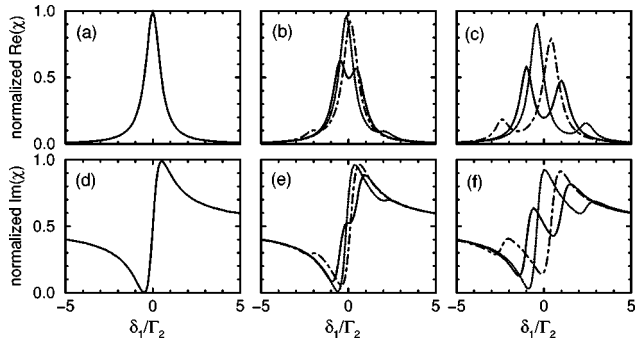

FIG. 3. Linear susceptibility χ as a function of δ_1/Γ_2 for $\delta_2/\Gamma_3=-2$ (dotted), 0 (solid), and 2 (dot-dashed). All parameters are the same as those for Fig. 2, except that $q_2=20$.

χ becomes similar to that of a bound-state system. As stated in Sec. I, we would like to point out once again that, for a bound three-level system it would be necessary to introduce an incoherent pumping in order to create a large refractive index at a zero-absorption point. When an autoionizing state with a proper q_1 value is employed as an upper state, however, neither third level, additional lasers, nor incoherent pumping is necessary to realize an enhanced index of refraction while canceling the absorption. As the intensity of the second laser is increased, the profile of χ begins to show a double-peak structure. The shape of each peak, however, is very different from each other due to the intrinsic coherence [Figs. 2(b) and 2(e), and 2(c) and 2(f)]. For comparison, corresponding results for $q_1=1$ and $q_2=20$ are shown in Fig. 3, from which we see that the profile of χ is affected not only by the value of q_1 but also by that of q_2, and as q_2 becomes large, the shapes of both peaks become more resemble. Calculations have been repeated for $q_1=20$ and $q_2=20$ (not shown in this paper), which exhibit the variation of the refractive index and the absorption profiles very similar to the one for a bound three-level system, as expected.

B. Ionization spectra

Having examined the variation of the linear susceptibility, we now move on to calculate ionization spectra into each continuum associated with each autoionizing state. In reality there may be more than one continua for each autoionizing state, but our model would be most convenient to understand the basic physics underlying this system. In order to explore the possibility of increasing the excitation efficiency to the HAS by controlling the laser detunings and intensities, we examine two cases, depending on the value of the normalized detuning δ_1/Γ_2: In the first case, the first laser is tuned to the *absorption minimum* of the LAS at $\Omega_2=0$ [12]. As the value of Ω_2 is increased, R_2 naturally increases. In the second case, the first laser is tuned to the *absorption maximum* of LAS at $\Omega_2=0$. Naively we expect that R_1, $R_2\sim 0$ for the first case and $R_1\gg R_2$ for the second case, independent of the values of Ω_1, Ω_2, and δ_2. It turns out, however, that it is not so simple as we show some results below.

We plot in Fig. 4 the ionization yields R_1 and R_2 as a function of normalized detuning δ_2/Γ_3 for $q_1=1$ and $q_2=2$ at fixed $\Omega_1=0.01\ \Gamma_2$ but different Ω_2's. In Fig. 4(a) $\Omega_2=0.1\Gamma_3$, while in Fig. 4(b) $\Omega_2=\Gamma_3$. For simplicity, the autoionization widths have been assumed to be the same, i.e.,

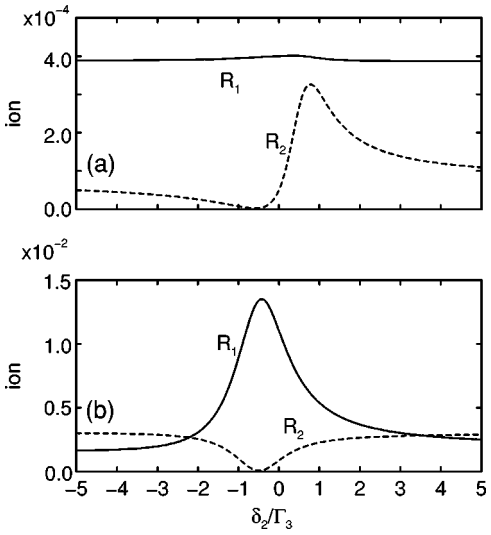

FIG. 4. Ionization yields R_1 (solid) and R_2 (dashed) as a function of δ_2/Γ_3. $\Gamma_2=\Gamma_3=1$, $\Omega_1=0.01\ \Gamma_2$, square pulse duration $T=20\ \Gamma_2^{-1}$, and $q_1=1$ and $q_2=2$ for all graphs. The first laser is tuned to the *absorption minimum*, i.e., $\delta_1/\Gamma_2=-0.5$. For (a) $\Omega_2=0.1\ \Gamma_3$, and for (b) $\Omega_2=\Gamma_3$.

$\Gamma_2=\Gamma_3=1$, and a square pulse has been employed with duration of $T=20\Gamma_2^{-1}$. Note that in Fig. 4, the first laser has been tuned to the absorption minimum of the LAS, i.e., $\delta_1/\Gamma_2=-q_1/2$, which is -0.5 in this particular case. Since the first laser is tuned to the absorption minimum, R_1 is very small in Fig. 4(a) at any δ_2/Γ_3, while R_2, although even smaller, shows an asymmetric profile, which is basically determined by the value of q_2. For larger Ω_2 [Fig. 4(b)], however, completely different ionization profiles emerge: The profile of R_1 is almost symmetric, while that of R_2 exhibits a minimum near $\delta_2/\Gamma_3\sim -0.5$ where R_1 is maximum. Calculations have been repeated under the moderately strong pumping condition of $\Omega_1=0.2\Gamma_2$ (not shown), and we find that the behavior of R_1 and R_2 is qualitatively similar to that shown in Fig. 4. The next question is how much the results depend on the value of q_2. In Fig. 5 we plot the results of similar calculations for $q_2=20$, with q_1 and all other parameters fixed to the same ones with those used to obtain Fig. 4. Again we see that the profile of R_1 is similar to that shown in Fig. 4, while that of R_2 reflects the value of q_2, except that in Fig. 5(b), both R_1 and R_2 exhibit maxima at about the same δ_2/Γ_3. Calculations have been repeated for the second case where the first laser is tuned to the absorption maximum of LAS at $\Omega_2=0$, i.e., $\delta_1/\Gamma_2=1/2q_1$, which is 0.5 in this particular case. The results are shown in Fig. 6 for $q_1=1$, $q_2=20$, and $\Omega_1=0.01\Gamma_2$, to be compared with Fig. 5. In Fig. 6(a), $R_1\gg R_2$, as expected. Namely, ionization from the LAS occurs before an atom is further excited to the HAS. It should be noted that a maximum of R_2 appears at the detuning where R_1 is minimum in Fig. 6(b).

Now we need to seek for a consistent interpretation for the results shown in Figs. 4–6. We find that this is attributed to the ac Stark splitting caused by the second laser: According to Eq. (11), $\sigma_{21}^{(1)}$ begins to exhibit a double-peak structure as the Rabi frequency Ω_2 increases. This has been illustrated in Figs. 2 and 3. Recalling that the depletion rate of the

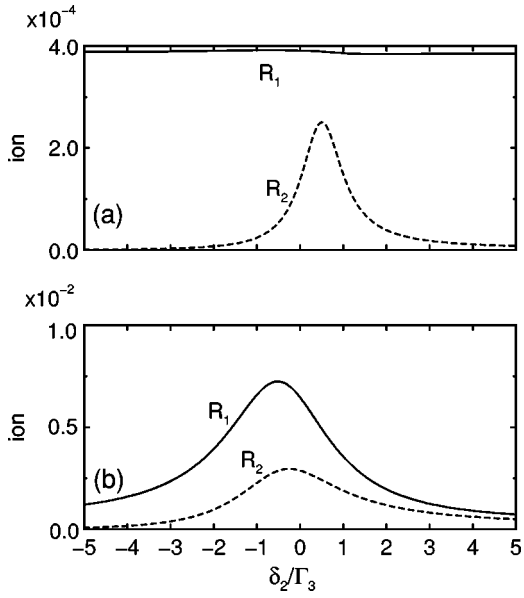

FIG. 5. Ionization yields R_1 (solid) and R_2 (dashed) as a function of δ_2/Γ_3. All parameters are the same as those for Fig. 4 except that $q_2=20$.

population of $|1\rangle$, or total ionization rate, is reflected by $\sigma_{21}^{(1)}$ through the relation

$$|\dot{\sigma}_{11}| = \gamma_1 - 2\,\mathrm{Im}\left[\Omega_1\left(1-\frac{i}{q_1}\right)\sigma_{21}^{(1)}\right] \tag{29}$$

under weak pumping condition, there is no wonder that the depletion rate also exhibits a double-peak structure. By looking at Fig. 3(f) at $\delta_1/\Gamma_2=-0.5$ for the curves of $\delta_2/\Gamma_3=-2$, 0, and 2, we see that the total ionization rate has a maximum near $\delta_2/\Gamma_3\sim 0$. This explains why R_1 in Figs. 4(b) and 5(b) show peaks near $\delta_2/\Gamma_3\sim 0$. Similar argument

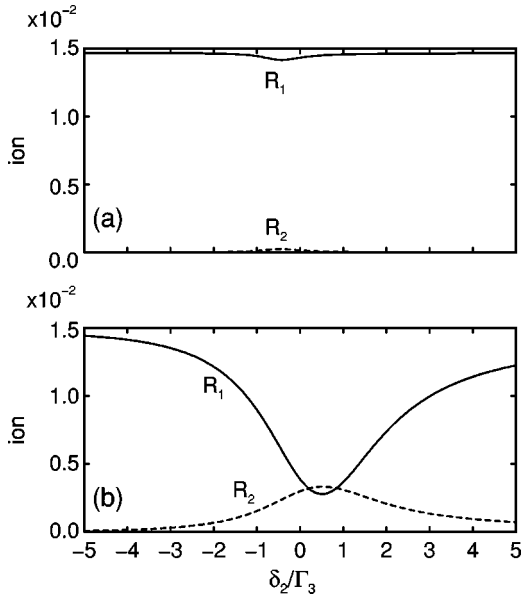

FIG. 6. Ionization yields R_1 (solid) and R_2 (dashed) as a function of δ_2/Γ_3. The first laser is tuned to the *absorption maximum*, i.e., $\delta_1/\Gamma_2=0.5$. All parameters are the same as those for Fig. 4 except that $q_2=20$.

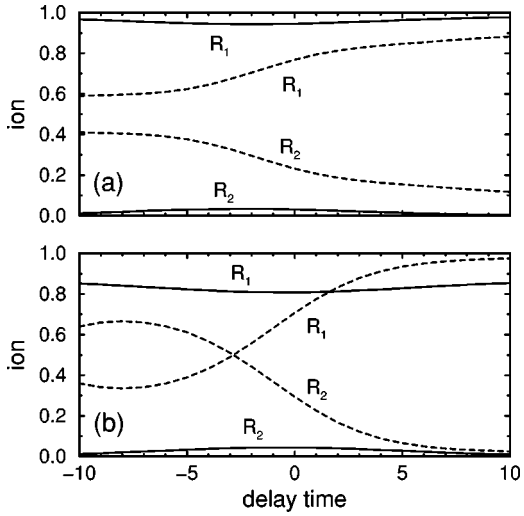

FIG. 7. Ionization yields R_1 and R_2 as a function of temporal pulse delay in units of Γ_2^{-1}. Negative delay means that the second laser precedes the first laser, i.e., counterintuitive pulse delay. (a) $q_1=1$ and $q_2=2$, and (b) $q_1=3$ and $q_2=5$. $\Gamma_2=\Gamma_3=1$, $\Omega_1=\Omega_2=\Gamma_2$, and the pulse duration $T=10\ \Gamma_2^{-1}$ (Gaussian FWHM) for both graphs (a) and (b). In (a), $\delta_1/\Gamma_2=0$ and $\delta_2/\Gamma_3=0$ (solid), and $\delta_1/\Gamma_2=-2$ and $\delta_2/\Gamma_3=2$ (dashed), while in (b), $\delta_1/\Gamma_2=0$ and $\delta_2/\Gamma_3=0$ (solid), and $\delta_1/\Gamma_2=-2$ and $\delta_2/\Gamma_3=2$ (dashed).

holds for the case in which the first laser is tuned to the absorption maximum [Fig. 6(b)]: see Fig. 3(f) at $\delta_1/\Gamma_2=0.5$. As for R_2, its shape is basically determined by the value of q_2 and the Rabi frequency Ω_2: If q_2 is small ($q_2=2$ in our case), the shape of R_2 is asymmetric with respect to δ_2/Γ_3 for small Ω_2. As Ω_2 becomes large, however, a saturation takes place as reported in Ref. [11], and a dip shows up near resonance. Note that the appearance of a dip instead of a peak is due to the presence of intrinsic coherence. If q_2 is large ($q_2=20$ in our case), the profile of R_2 is almost symmetric with a peak near resonance, and as Ω_2 becomes large the profile becomes broader but does not change the shape. A dip does not appear for large q_2, since the intrinsic coherence is not sufficiently large.

C. Effects of the pulse delay

In order to avoid an additional complexity which might hinder the physical understanding of this system, we have not so far introduced a temporal delay between two pulses. Having understood the basic behavior of the system, we are now ready to focus on the effects of the pulse delay. Representative results are shown in Figs. 7(a) and 7(b) for $q_1=1$ and $q_2=2$, and $q_1=3$ and $q_2=5$, respectively. Negative delay indicates that the second laser precedes the first laser, i.e., counterintuitive pulse delay. The temporal shape of both pulses has been assumed to be Gaussian with $T=10\ \Gamma_2^{-1}$ full width at half maximum (FWHM) and $\Gamma_2=\Gamma_3=1$, and $\Omega_1=\Omega_2=\Gamma_2$ for all graphs in Figs. 7(a) and 7(b). It can be seen that the choice of the detunings is very important for efficient excitation to the HAS. Our results demonstrate that the counterintuitive pulse sequence is effective even when not only the intermediate but also the final states are autionizing states. By comparing Figs. 7(a) and 7(b), it can also be seen that the effect of the pulse delay is qualitatively similar

regardless of the values of q_1 and q_2, as long as q_1 and q_2 are not very large, but that the amount of the effect depends on the *detunings*. In this particular case, the pulse delay effect is more effective when the detunings are nonzero. Generally speaking, this is not very surprising, since there is intrinsic coherence which causes an interference around an autoionizing resonance, leading to the asymmetric ionization profile as can be seen in Figs. 4–6. For an autoionizing system, the intrinsic coherence competes with the laser-induced coherence. Therefore the behavior of the system involving an autoionizing state(s) might be quite different in some respects, with/without pulse delay, from the system consisting of bound states only, while still possessing some similarities to the bound state system. It should be noted that the pulse delay may not be necessarily important for efficient excitation to the higher continuum: Rather, a proper choice of the detunings would be more important in some cases, as shown in Fig. 7(b). The last remark we would like to make is that, in contrast to a bound three-level system, the two-photon resonance condition is not so important in this system for efficient excitation to the HAS. This would be due to the fact that the HAS, as well as the LAS, is significantly broadened by autoionization.

IV. CONCLUSIONS

In conclusion, we have studied the influence of strong coupling and pulse delay in a system involving double autoionization resonance. In particular, we have focused on the variation of the linear susceptibility, ionization spectra into each continuum for different detunings and laser intensities, and pulse delay effects in terms of the ionization yield. We have derived an expression for the linear susceptibility, and presented a few numerical examples. When both of the asymmetric parameters q_j $(j=1,2)$ are large, the profile of the linear susceptibility does not differ so much from that for a bound three-level system, as expected. For smaller values of q_j $(j=1,2)$, however, both the real and the imaginary parts of the susceptibility exhibit strong asymmetries as the laser detunings and intensities are varied. As for the ionization spectra, it has been found that the ac Stark splitting plays an important role when the Rabi frequency Ω_2 due to the second laser becomes comparable to the larger of the autoionization widths Γ_2 and Γ_3. Namely, when $\Omega_2 \ll \Gamma_2, \Gamma_3$, ac Stark splitting is negligible, and by tuning the first laser to the absorption minimum of the LAS, a selective excitation to the HAS can be achieved. Note, however, that this is true only if $|q_1|$ is not very small: If $|q_1|$ is ~ 1 or smaller, lots of atoms will be lost directly into the continuum associated with the LAS, and hence the process is not so selective. When the second laser becomes intense such that Ω_2 is comparable to the larger of Γ_2 and Γ_3, ac Stark splitting shifts the position of the absorption minimum, and it turned out to be essential for efficient excitation to the HAS to detune the first laser from the absorption minimum at $\Omega_2 = 0$. When both lasers are intense, the system behavior is complicated and it is not easy to make even qualitative remarks. Last of all, the effects of the temporal delay between two pulses have also been investigated. We have found that the proper choice of the detunings and counterintuitive temporal delay can lead to the significant enhancement of excitation to the higher continuum state.

[1] G. Alzetta, A. Gozzini, L. Moi, and G. Orrios, Nuovo Cimento Soc. Ital. Fis., B **36**, 5 (1976).
[2] A. Aspect, E. Arimondo, R. Kaiser, N. Vansteenkiste, and C. Cohen-Tannoudji, Phys. Rev. Lett. **61**, 826 (1988).
[3] S.E. Harris, Phys. Rev. Lett. **62**, 1033 (1989).
[4] K.-J. Boller, A. Imamoglu, and S.E. Harris, Phys. Rev. Lett. **66**, 2593 (1991).
[5] K. Bergmann, H. Theuer, and B.W. Shore, Rev. Mod. Phys. **70**, 1003 (1998).
[6] B. Dai and P. Lambropoulos, Phys. Rev. A **36**, 5205 (1986).
[7] P.L. Knight, M.A. Lauder, and B.J. Dalton, Phys. Rep. **190**, 1 (1990).
[8] Takashi Nakajima and P. Lambropoulos, Opt. Commun. **118**, 40 (1995).
[9] S.L. Shao, D. Charalambidis, C. Fotakis, Jian Zhang, and P. Lambropoulos, Phys. Rev. Lett. **67**, 3669 (1991).
[10] S. Cavalieri, F.S. Pavone, and M. Matera, Phys. Rev. Lett. **67**, 3673 (1991).
[11] P. Lambropoulos and P. Zoller, Phys. Rev. A **24**, 379 (1981).
[12] T.F. Gallagher, R. Kachru, N.H. Tran, and H.B. van Linden van den Heuvell, Phys. Rev. Lett. **51**, 1753 (1983).
[13] Jian Zhang and S.J. van Enk, Phys. Rev. A **52**, 4640 (1995).
[14] N.E. Karapanagioti, O. Faucher, Y.L. Shao, D. Charalambidis, H. Bachau, and E. Cormier, Phys. Rev. Lett. **74**, 2431 (1995).
[15] N.E. Karapanagioti, D. Charalambidis, C.J.G.J. Uiterwaal, C. Fotakis, H. Bachau, I. Sánchez, and E. Cormier, Phys. Rev. A **53**, 2587 (1996).
[16] M.O. Scully, Phys. Rev. Lett. **67**, 1855 (1991).
[17] M.O. Scully and Shi-Yao Zhu, Opt. Commun. **87**, 134 (1992).
[18] M. Fleischhauer, C.H. Keitel, M.O. Scully, Chang Su, B.T. Ulrich, and Shi-Yao Zhu, Phys. Rev. A **46**, 1468 (1992).
[19] Takashi Nakajima, M. Elk, J. Zhang, and P. Lambropoulos, Phys. Rev. A **50**, R913 (1994).
[20] Takashi Nakajima and P. Lambropoulos, Z. Phys. D **36**, 17 (1996).
[21] V.S. Malinovsky and D.J. Tannor, Phys. Rev. A **56**, 4929 (1997).
[22] Takashi Nakajima, Phys. Rev. A **59**, 559 (1999).
[23] N.V. Vitanov, B.W. Shore, and K. Bergmann, Eur. Phys. J. D **4**, 15 (1998).
[24] M.N. Kobrak and S.A. Rice, Phys. Rev. A **57**, 2885 (1998).